EPJ Web of Conferences **314**, 00040 (2024) https://doi.org/10.1051/epjconf/202431400040
QCD@Work 2024

Holographic phases of QCD

Akash Singh[1,*] and *K.P.* Yogendran[1,**]

[1]Department of Physical Sciences, IISER Mohali, Sector 81, Knowledge City, Punjab, 140306, India

Abstract. In this presentation, we will discuss the QCD phase diagram at finite temperature and finite baryon chemical potential using a hardwall holographic AdS/QCD model. We study bulk gravity solutions with appropriate boundary conditions that represent strongly interacting nuclear matter, deconfined quarks, and various possible condensates over a range of baryon chemical potential and temperature.

1 Introduction

The QCD phase diagram involves a variety of phases in the spectrum of temperature and baryon chemical potential. These phases can be observed in the form of hadrons (baryons and mesons) in the gaseous and liquid phases under low to intermediate conditions. In extreme conditions, they manifest as the quark-gluon plasma in heavy-ion collisions at very high temperatures, or as baryonic pairs (superconductors/superfluids), meson condensates, or quark pairs inside neutron stars at supranuclear densities [1]. However, it is challenging to compute the properties of the matter in these phases due to the strong nature of interactions among the constituents at low energies and/or low temperatures.

Lattice QCD has demonstrated its importance as a tool for making predictions at finite temperatures and zero chemical potential. However, it encounters limitations at finite chemical potentials due to the infamous sign problem. Alternatively, effective field theories such as chiral perturbation theory, the Nambu-Jona-Lasinio (NJL) model, the Hadron Resonance Gas (HRG) model, and others rely heavily on approximations, resulting in constrained regions of validity.

A modern method for understanding the QCD phase diagram is based on the AdS/CFT correspondence. There are two main approaches: top-down and bottom-up. The top-down approach is rooted in string theory, whereas the bottom-up approach is more phenomenological. Some examples of the top-down approach are the D3/D7 setup and the Witten-Sakai-Sugimoto models. The bottom-up approach includes Hardwall models, Softwall models, VQCD models, and more. The hardwall AdS/QCD holography has mostly been limited to the finite density *deconfined* phases, lacking a description of a finite density confined phase. In our work, we focus on a family of background geometries in a 5-dimensional hardwall framework, which we call the charged AdS geometry (CAdS). These have nonzero electric fields but do not have a black hole.

In section 2, we describe our 5-dimensional hardwall model. The possible solutions are discussed in section 3. We detail the phase diagram in the $\mu - T$ plane that we obtain with

*e-mail: akashsingh@iisermohali.ac.in
**e-mail: yogendran@iisermohali.ac.in

different choices of boundary conditions in section 4. Section 5 study the probe baryonic condensates. We conclude with a discussion and future directions in section 6.

2 Holographic hardwall model

The hardwall model is based on imposing an IR cutoff in the bulk radial coordinate. This breaks the conformal symmetry and enables the possibility of a confinement-deconfinement transition [2]. This work focuses on transitions from confining geometries to deconfining geometries at finite chemical potential. In this section, we discuss a 5-D holographic hardwall model based on AdS/QCD models. The model incorporates a bulk metric field $g_{\mu\nu}$, which is dual to the conserved boundary stress-energy tensor T_{ij} (here $\mu, \nu = (x_0, x_1, x_2, x_3, z)$ and i, j restricted to boundary directions only). The model also includes a $U(1)$ gauge field A_μ corresponding to the conservation of the baryon number in boundary theory (or the global $U(1)_B$ symmetry). Therefore, the minimally coupled Einstein-Maxwell action with Gibbons-Hawking and the boundary counter term in 5-dimensions is

$$S = \frac{N_c^2}{8\pi^2 L^3}\int d^5x\,\sqrt{g}\,(R - 2\Lambda) - \frac{\theta N_f N_c}{24\pi^2 L}\int d^5x\,\sqrt{g}\frac{F^2}{4} - \frac{N_c^2}{4\pi^2 L^3}\int d^4x\,\sqrt{\gamma}\left(\Theta - \frac{3}{L}\right) \quad (1)$$

with N_f, N_c, and L are the number of flavors, colors and AdS radius, respectively. The cosmological constant in the Einstein-Hilbert part of the action is set to be $2\Lambda = -\frac{12}{L^2}$ so that the asymptotic solution is AdS_5. Here γ is the induced metric on the UV surface $z = \epsilon$, and Θ is the trace of the extrinsic curvature associated with this surface.

The parameter θ is a new idea that needs to be explained. It allows for different choices of the internal compactification manifold of the Dp-branes as well as dilaton couplings to the Dp-brane. The normalization we consider in the F^2 term is such that when $\theta = 6$, we get the Maxwell action by expansion of the DBI action for the D7-brane.

3 Solutions/phases

In order to simplify the equations of motion and derive solutions with the appropriate boundary conditions, the first crucial step is to carefully select an ansatz for the fields. We consider a diagonal metric ansatz,

$$ds^2 = -g(z)\frac{L^2}{z^4}dt^2 + \frac{L^2}{z^2}d\vec{x}^2 + \frac{L^2}{g(z)}dz^2 \quad (2)$$

which implies that the (conformal) boundary is at $z = 0$. This ansatz respects the translational and rotational symmetry of the phases in which we are interested. The gauge field ansatz is $A_0 = \phi(z)$, $A_i = 0$ where $i = 1, 2, 3$ with gauge condition $A_z = 0$. The equations of motion with these ansatz are:

$$g'(z) - \frac{6g(z)}{z} + 4z - \zeta z^5\left(\frac{\phi'(z)^2}{2}\right) = 0\,; \qquad \phi''(z) - \frac{\phi'(z)}{z} = 0 \quad (3)$$

where the parameter $\zeta = \frac{\theta N_f}{9N_c}L^2$ controls the effect of the gauge field on the background (large N_c being the probe approximation).

There are three boundary conditions: one for g and two for ϕ. The functions $g(z)$ and $\phi(z)$ with suitable boundary conditions describe geometric solutions. There are three possible geometries:

1. **Thermal AdS:** zero density, confined phase.

$$g(z) = z^2 \; ; \qquad \phi(z) = \mu \tag{4}$$

2. **Charged Black Hole:** finite density, deconfined phase.

$$g(z) = z^2\left(1 - cz^4 + \frac{\zeta\mu^2}{z_H^4 L^2}z^6\right) \; ; \qquad \phi(z) = \mu\left(1 - \frac{z^2}{z_H^2}\right) \tag{5}$$

where z_H is the black hole horizon. The parameter c is fixed by the condition that z_H is the smallest root of $g(z_H)$ for each μ (quark chemical potential).

3. **Charged AdS:** finite density, confined phase.

The charged AdS is an overcharged horizonless geometry in the bulk that represents a finite-density confined phase of the boundary theory [3].

$$g(z) = z^2\left(1 - cz^4 + \frac{\zeta Q}{L^2}z^6\right) \; ; \quad \phi(z) = \pm\mu + Qz^2; \tag{6}$$

with $\frac{\zeta^2 Q^4}{L^4 c^3} > \frac{4}{27}$ implying that the function $g(z)$ never has a root. Here, Q and c (or equivalently, $g(z_0)$) are free parameters that have to be fixed to completely determine the solutions. In Section 4, we will discuss the possible choices of boundary conditions to fix these parameters.

The thermodynamic quantities for these geometric phases (as shown in Table 1) can be obtained as follows: Finite quark chemical potential $\mu_Q = \mu = \frac{\mu_B}{N_c}$ as the non-normalizable mode of the gauge field $\phi(z)$. Following [2] or [4], we can set the temperature of the thAdS and CAdS to any finite value, the temperature in CBH is fixed by the regularity of the metric near the horizon, the pressure is computed using the Euclidean on-shell action,

Table 1. Thermodynamic Quantities.

	ThAdS	**CBH**	**CAdS**
Chemical potential	$\phi(\epsilon)$	$\phi(\epsilon)$	$\phi(\epsilon)$
Temperature	T	$\frac{1}{\pi z_H}\left\|1 - \frac{\zeta\mu^2 z_H^2}{2L^2}\right\|$	T
Pressure	$\frac{N_c^2}{4\pi^2 z_0^4}$	$\frac{N_c^2}{8\pi^2}\left(\frac{1}{z_H^4} + \frac{\zeta\mu^2}{z_H^2 L^2}\right)$	$\frac{N_c^2}{8\pi^2}\left(\frac{z_0^2 + g(z_0)}{z_0^6}\right)$

4 Boundary conditions and phase diagram

In CAdS geometries, we need to determine the boundary conditions at the IR cutoff that will result in equations of state. These different boundary conditions significantly change the boundary theory phases and, thus, the phase diagram.

4.1 A simple boundary condition

A simple choice of boundary conditions on the gauge field is to set $\phi(z_0) = 0$ which leads to an equation of state $Q(\mu) = \frac{\mu}{z_0^2}$. The other boundary condition $g(z_0)$ (or $\bar{g_0}$) is fixed via the

ρ-meson mass as a normalizable (isospin) gauge field plane wave fluctuation. For a detailed discussion, see [3].

This allows us to extend the confinement/deconfinement phase transition of [2] in the finite chemical potential region. At $T = 0$, the deconfined phase is preferred for a large chemical potential, as described by the following inequality,

$$\left(\frac{\mu\alpha_g}{M_g}\right)^2 > \frac{6N_c}{\theta N_f}\left(1 + \sqrt{4 + 3\alpha_\rho\left(\frac{M_\rho}{\alpha_g M_g} - 1.766\right)^4}\right) \tag{7}$$

where α_g and α_ρ are numerical constants.

4.2 Physically motivated boundary condition

Next, we will explore the IR boundary conditions such that the hardwall model represents the equation of state of a baryonic system at low to intermediate densities as determined by the effective field theory (EFT) methods.

That is to say, we choose $g(z_0)$ (and $\phi(z_0)$), so that the pressure (and the number density) is the pressure (and the number density) of baryonic degrees of freedom computed by EFT techniques.

$$\rho = \frac{\theta N_f N_c}{12\pi^2} Q\,; \qquad g(z_0) = \bar{g}_0 + \frac{8\pi^2}{N_c^2}\left(p - \frac{2\pi^2 z_0^2}{\theta N_f N_c}\rho^2\right) \tag{8}$$

At low densities, a gas of interacting baryons might be described by in-medium chiral perturbation theory with the Van der Waals type phase [5]. At higher densities and/or temperatures, nuclear physics suggests the appearance of a quarkyonic phase, which is described by the two-flavor NJL model [6]. Therefore, we chose these descriptions and compared them with the deconfined (CBH) phase to obtain the phase diagram.

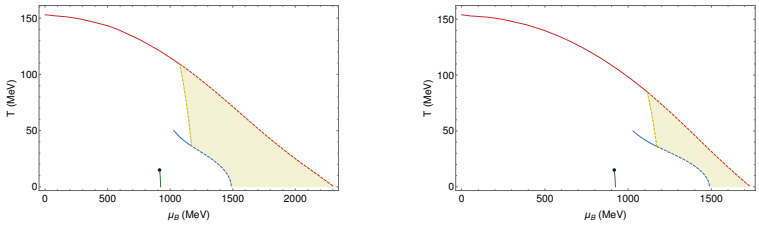

(a) $\zeta = 0.77$, $g_0 = 6$ (b) $\zeta = 1$, $g_0 = 6$

Figure 1. Phase diagram in $\mu - T$ plane for two different values of ζ.

The phase diagram for physical IR boundary conditions with van der Waals and quarkyonic phases is shown in figure 1. The van der Waals type phase is favored at low density. A liquid-gas phase transition represented by a solid green line exists, which ends at a critical point. As the chemical potential increases, the van der Waals phase makes a transition to the quarkyonic phase at intermediate density (blue line). Since the vdW description is valid only up to $T \sim 50$ MeV, we do not extend this coexistence line further. The quarkyonic matter melts into a deconfinement phase (charged black hole) at high densities (shown by the red line). The yellow region marks a phase where the chiral condensate σ vanishes indicated by $\frac{\sigma(T,\mu)}{\sigma(0,0)} < 0.1$.

5 Baryonic condensate solutions

The AdS/CFT dictionary allows us to map the nonzero vev of a condensate operator with the scaling dimensions Δ to a non-trivial massive complex scalar field profile without a node and vanishing non-normalizable mode. Therefore, further developing our idea, we include a complex scalar field ψ charged under $U(1)_B$. This scalar field is dual to the baryon condensate given the charge q of the field in the bulk and the scaling dimension of the condensate operator Δ in the boundary. The action for the Einstein-Maxwell-Scalar system with appropriate counter terms is,

$$S = S_0 - \lambda_s \int d^5x \sqrt{g}\left(|D\psi|^2 + m^2|\psi|^2\right) - \lambda_s \int d^4x \sqrt{\gamma}\frac{d-\Delta}{2L}|\psi|^2 \tag{9}$$

where S_0 is given in (1). The equation of motion for the scalar field in the *confined* backgrounds discussed in section 3 is,

$$\psi''(z) + \psi'(z)\left(-\frac{5}{z} + \frac{g'(z)}{g(z)}\right) - \left(\frac{m^2}{g(z)} - \frac{q^2 z^4 \phi(z)^2}{g(z)^2}\right)L^2\psi(z) = 0 \tag{10}$$

At the on-set of condensation, the scalar field will have small amplitude. Therefore, the on-set of condensation can be reliably estimated by studying the scalar field in the probe approximation. An interesting outcome of the probe analysis in CAdS geometries (at $T = 0$) is the vanishing of the condensate at high density signaled by the node appearing for the scalar field profile as shown in figure 2

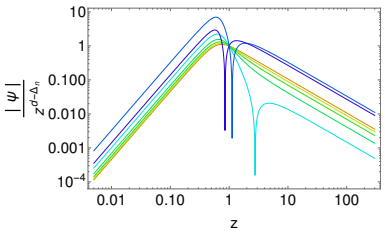

Figure 2. Extended absolute scalar field solution in a LOGLOG plot in the NJL phase. Different colors represent varying values of μ, with orange indicating the lowest and violet the highest.

It should be noted that in these cases, the value of the scalar field at the IR cutoff is being held fixed. The table 5 shows the on-set and off-set of the condensates in the Van der Waals and NJL phase in the probe approximation.

Table 2. The on-set and off-set of condensate.

Phase	Δ	q	**sign**	**On-set μ (MeV)**	**Off-set μ (MeV)**
VdW	4	6	-ve	1096.2	1139.7
VdW	4.25	6	-ve	1218.0	1261.5
VdW	4.5	6	-ve	1331.1	1374.6
NJL	3	2	+ve	1722.6	1914.0

The choice of q and Δ in the NJL phase is justified because the boundary condensate operator is expected to be composed of two quark fields in the quarkyonic phase. In contrast, in the VdW phase, the charge is $2N_c$, but the scaling dimension does not need to be $3N_c$ due to anomalous dimension corrections. Therefore, we show condensation in the VdW phase for a few values of Δ. It is noteworthy that the on- and off-set is shifting; however, the difference is always $\simeq 40$ MeV.

In an upcoming study, a comprehensive analysis of condensates with different values of Δ in the VdW phase and backreacted solutions will be presented.

6 Conclusion and Discussion

A simple 5-D holographic hardwall model provided low density confined phase, resulting in a complete phase diagram. By implementing the physical IR boundary conditions, we were able to match equations of state with the low density effective field theory results. The probe analysis of baryon condensates in the confined phase at zero temperature identifies a critical chemical potential beyond which the condensate disappears. The study for backreacted condensate solutions with physical boundary conditions is ongoing. The backreaction of the scalar field leads to a new set of boundary conditions at the IR cutoff, which results in interesting outcomes. The enhancement of the model by incorporating isospin and chiral condensate will be interesting for the QCD phenomenology. Another interesting question is to construct a top-down D3/D7 hardwall framework in 10-D with backreaction that could provide a finite density confined phase with baryons as solitons localized behind the cutoff.

References

[1] C. J. Pethick, T. Schaefer and A. Schwenk, "Bose-Einstein condensates in neutron stars," [arXiv:1507.05839 [nucl-th]]

[2] C. P. Herzog, "A Holographic Prediction of the Deconfinement Temperature," Phys. Rev. Lett. **98** (2007), 091601 doi:10.1103/PhysRevLett.98.091601 [arXiv:hep-th/0608151 [hep-th]]

[3] A. Singh and K. P. Yogendran, "Confined phases at finite density in the Hardwall model," [arXiv:2408.10986 [hep-th]]

[4] A. Singh and K. P. Yogendran, "Phases of a 10-D holographic hard wall model," JHEP **02** (2023), 168 doi:10.1007/JHEP02(2023)168 [arXiv:2208.09387 [hep-th]]

[5] S. Fiorilla, N. Kaiser and W. Weise, "Chiral thermodynamics of nuclear matter," Nucl. Phys. A **880** (2012), 65-87 doi:10.1016/j.nuclphysa.2012.01.003 [arXiv:1111.2791 [nucl-th]]

[6] S. P. Klevansky, "The Nambu-Jona-Lasinio model of quantum chromodynamics," Rev. Mod. Phys. **64** (1992), 649-708 doi:10.1103/RevModPhys.64.649